

RESEARCH

Open Access



# Antitumor efficiency and photostability of newly green synthesized silver/graphene oxide nanocomposite on different cancer cell lines

Amna H. Faid<sup>1\*</sup>, M. Abdel Rafea<sup>2,3</sup>, Sara Gad<sup>3</sup>, Marwa Sharaky<sup>4,5</sup> and Marwa A. Ramadan<sup>6</sup>

\*Correspondence:  
amna.hussein@cu.edu.eg

<sup>1</sup> Department of Laser Science and Interaction, National Institute of Laser Enhanced Science (NILES) Cairo University, Giza, Egypt

<sup>2</sup> College of Science, Department of Physics, Imam Mohammad Ibn Saud Islamic University (IMSIU), Riyadh 11623, Kingdom of Saudi Arabia

<sup>3</sup> Electronic Materials Research Department, Advanced Technology and New Materials Research Institute, City of Scientific Research and Technological Applications (SRTA-City), Alexandria, Egypt

<sup>4</sup> Pharmacology Unit, Cancer Biology Department, National Cancer Institute (NCI), Cairo University, Giza, Egypt

<sup>5</sup> Biochemistry Department-Faculty of Pharmacy, Ahram Canadian University, Giza, Egypt

<sup>6</sup> Department of Laser Application in Metrology, Photochemistry and Agriculture, National Institute of Laser Enhanced Science (NILES) Cairo University (CU), Giza, Egypt

## Abstract

It is crucial to enhance new compounds for the treatment of most malignancies, and graphene oxide/silver nanocomposite (GO/Ag NC) has been paying attention to biomedical applications such as malignancies. In this work, green synthesized Ag@Cht NPs were successfully produced using chitosan for reduction and stabilization and added on GO sheet forming novel GO/Ag NC. Then, the produced anticancer nanomaterials GO, Ag@Cht NPs, and GO/Ag NC were assessed for their cytotoxicity against four distinct cancer cell lines: H460, HCT116, MDA-MB-468, and FaDu cells, at varying concentrations, using SRP assay after 48 h. The prepared nanomaterials were characterized by TEM, UV–Vis spectrophotometry, FTIRs, Raman spectroscopy and XRD. TEM images showed a regular spread of Ag@Cht NPs on the GO sheets with an average particle size of 15 nm. UV–Vis spectrophotometry shows two main characteristic peaks for GO/Ag NC, one close to 230 nm corresponds to GO, while the other peak at 425 nm due to Ag@Cht decorating the GO surface was blue shifted by few nanometers from 427 nm for Ag@Cht. Results of the laser irradiation by DPSS (diode-pumped solid state) confirm the photothermal stability of the prepared nanocomposite as there is no change in surface plasmon resonance (SPR) with varying exposure time. FTIRs measurements indicate that Ag ions interact with a hydroxyl group. This interaction shifts the O–H wavenumber and decreases the bond stretching intensity. In addition, Ag@Cht NPs and Ag/GO NC showed enhanced activity against cancerous cells. Results showed that GO, Ag@Cht NPs, and GO/Ag NC at (200, 400, and 600 µg/ml) had an impact on all evaluated cell lines. In MDA-MB-468, HCT116, H460, and FaDu cells, Ag@Cht NPs had the most effect across all employed cell lines, with IC<sub>50</sub> values of 5.5, 9, 6, and 7.75 µg/ml, respectively. In conclusion, the produced novel nanocomposite may be an effective way to treat different cell lines, and future work is to use the prepared nanomaterials as anticancer drug delivery in photothermal chemotherapy combination treatment.

**Keywords:** Graphene oxide–silver nanoparticles nanocomposites, Laser photostability, Cytotoxicity, Different cell lines



## Introduction

The advance of nanotechnology, which suggests incredible ways to overcome deadly diseases, has enhanced progression in biomedical science. It is essential to find a treatment for cancer, which has a major hazard to human life and health (Faid et al. 2022a, 2023; Ramadan and El-Tayeb 2023; Mohamad et al. 2023a). Although traditional therapeutic approaches have achieved a lot, their clinical applicability is still constrained by issues such the multidrug resistance (MDR) impact, non-specific biodistribution and low bioavailability (Yan et al. 2020; Faid et al. 2022b; Alexeree et al. 2024; Ramadan et al. 2024). New techniques are made possible by the use of nanomaterials that hold tremendous promise for the treatment of cancer in order to increase the safety and efficacy of tumor therapy such as biopolymers and nanostructures that are derived from natural and bio renewable resources. Several resources have been utilized for these purposes such as proteins, lipids, lignin, hyaluronic acid, starch, cellulose, gum, pectin, alginate, chitosan, chitosan gold nanoparticles (AuNPs) and silver nanoparticles (Ramadan et al. 2024, 2022; Carrion et al. 2021). At present, NPs/NCs are being synthesized via three main ways: physical, chemical, and green methods. Scientists are now mentioning that the green method of NPs/NC synthesis is the best method because of its facile processing, use of nontoxic chemicals, and low cost. The reducing and capping agents have important roles in the preparation of NPs/NCs. Highly toxic chemicals/solvents used in physical and chemical methods of NPs/NCs synthesis are responsible for environmental dangers thus restricting its application in medical and clinical fields. Therefore, the green method eliminates the use of expensive chemicals, consumes less energy, and produces eco-friendly NPs/NCs. However, it is still challenging to develop a simple, rapid, and inexpensive green protocol for the synthesis of NPs/NCs with extremely effective anticancer performance (Ahamed et al. 2021). Graphene oxide (GO)-based nanomaterials are two-dimensional architectures that have attracted a lot of scientific interest due to its special qualities of high chemical–mechanical stability and biocompatibility. Mono- or multi-layers of GO nanosheets have carbon layers decorated with epoxide and hydroxyl groups. As a result of its exceptional characteristics, GO-constructed nanomaterials are used in various applications such as sensors (Mohamad et al. 2023a; Hong et al. 2010), anticancer (Ramadan et al. 2024; Liu et al. 2021; Loutfy et al. 2017), antibacterial (Mostafa et al. 2022), antiviral (Kumari et al. 2020), phototherapy and bioimaging (Alexeree et al. 2024). The deacetylation of chitin yields chitosan (CS), which is considered as one of the most remarkable, affordable, nontoxic, and biocompatible raw biomaterials that are found in mammals and crustaceans. Numerous uses of CS in biomedicine have been investigated in order to widely employ nanoparticles in many medicinal applications (Alexeree et al. 2024; Tao et al. 2020). Silver nanoparticles (Ag NPs) have a cytotoxic effect on cell viability and are primarily responsible for the anti-tumor and anticancer effects (Ali et al. 2022; Mohamad et al. 2023b). They also have a strong antibacterial action, besides in cutting-edge medical applications, such as bioimaging, bone healing, vaccine adjuvants, and wound-healing agents (Xu et al. 2020). The anticancer properties of AgNPs have been proven in many previous studies. AgNPs can disrupt the cellular communication network but fault cell signaling. In addition, AgNPs can cause DNA damage, increase the expression of molecular protein caspase, and start cellular apoptosis. The ability to cause apoptosis makes them essential in cancer

treatment (Motafeghi et al. 2023). A spontaneous aggregation effect occurs on Ag NPs due to high active surface and such aggregation can be prevented by supporting carrier such as graphene oxide sheet which let AgNPs surface be more active. GO can stop AgNPs from aggregating, and the AgNPs, which immobilized on the outward of the GO nanosheet, can stop GO from aggregating. Graphene-based nanomaterials appear to be trustworthy due to simple processing, low production costs, and distinctive chemical and physical features (Lozovskis et al. 2020; Yousefi et al. 2017). Nanocomposites have distinct physicochemical characteristics that set them apart from other synthetic therapeutics (Sajjadi et al. 2021). There are numerous various types of nanocomposites that are frequently grouped based on their unique design and matrix type. In comparison to typical polymer composites and nanocomposites, they may be made with less processing effort and lighter component weights. In addition, the enhanced multifunctional properties made attainable by nanocomposites enable novel uses of polymer (Iravani and Varma 2020; Nasrollahzadeh et al. 2016). Metallic nanocomposites are classified as non-polymer-based and polymer-based nanocomposites (Salah et al. 2023). Metal/polymer nanocomposites have attracted a lot of attention owing to their wide range of potential applications. They were investigated extensively not only according to their adaptability and environmentally friendly but also according to their inherent biodegradability and biocompatibility (Raza et al. 2021). Silver nanoparticles (AgNPs) have received a lot of interest due to controllable particle size, the nanoparticle form and active surface area which has been employed for surface-enhanced Raman scattering. Supporting the nanoparticles on the graphene sheets keeps the surface to be active as a result from preventing of aggregation. Recently, graphene–silver nanocomposites have been synthesized by an environmentally friendly technique including microwave irradiation and techniques incorporating biomolecules such as gelatin, bacteria, tryptophan, and plant extracts. Because of their distinctive features and functionalities, the biomedical research is increasingly examining the potential of employing hybrid nanomaterials, such as GO/Ag NC, for anticancer (Ramadan et al. 2024; Lange et al. 2022), antibacterial, antimicrobial and sensing platform applications (Tramonti et al. 2022). In order to prevent aggregation of AgNPs and enabling for a regulated discharge of AgNPs<sup>+</sup> ions, AgNPs can be attached to the surface of GO sheets (Yuan et al. 2021). This research aims to study the anticancer effect of novel green synthesized GO/Ag NC on different cell lines. An environmentally eco-friendly production of silver nanoparticles (AgNPs) was synthesized by applying chitosan as a capping and reducing agent with subsequently loading on GO sheet forms GO/Ag NC. Moreover, the antitumor activities of the GO/Ag NC on human lung cancer cell line (H460), a human colon cancer cell line (HCT116), a human breast tumor cell line (MDA-MB-468), and a human hypopharyngeal cell line (FaDu) have been performed.

## **Material and methods**

### **Green synthesis of Ag@Cht NPs**

A variety of methods to generate silver nanoparticles have been developed due to the wide range of applications (Ramadan and El-Tayeb 2023; Alexeree et al. 2024; Ali et al. 2022). The most popular synthetic approach for making silver nanoparticles involves reducing a silver solution using a chemically reducing agent (Mohamad et al. 2023b;

Amin et al. 2009; Lou et al. 2006; Faid et al. 2022). The creation of a green synthesis for silver nanoparticles is required because such reducing agents could be linked to biological or environmental problems. As a result, Chitosan, a polysaccharide biopolymer made from naturally occurring chitin, exhibits special polycationic and film-forming capabilities because it contains functional groups with active amino and hydroxyl atoms (Ramadan et al. 2022; Ahmed and Badr 2018). With the view that using AgNPs in biomedical fields, we have tried to create AgNPs with nontoxic and biodegradable chitosan in the hopes that it will combine desirable qualities including environmental safety, low toxicity, and simple fabrication. Here, the environmentally friendly production of silver nanoparticles coated in chitosan, (Ag@Cht NPs) was proven as follows: 30 ml of chitosan solution (99.9%, Sigma-Aldrich) produced in 1% acetic acid and 3 ml of  $10^{-2}$  M AgNO<sub>3</sub> (99.9%, Sigma-Aldrich) were combined and agitated until completely homogeneous. The mixture was then put into a tiny brown bottle and left to stand at 95 °C for 12 h. Within hours of the reaction starting, the solution transformed from colorless to bright yellow, and then to yellowish brown. Following that, lyophilizer was used to dry the Ag@Cht NPs.

#### **Preparation of GO**

As mentioned in many previous literatures, GO nanosheets were synthesized by oxidation of natural graphite according to a modified Hummers method (Ramadan et al. 2024; Salah et al. 2023). Potassium permanganate KMnO<sub>4</sub> (99.9%, Sigma-Aldrich) of mass 3 g was added gradually to a mixture of 0.5 g graphite (99.9%, Alfa Aesar, Ward Hill, MA, USA), 25 ml sulfuric acid H<sub>2</sub>SO<sub>4</sub> (96%, H<sub>2</sub>SO<sub>4</sub>, Sigma-Aldrich, St. Louis, MO, USA), and 0.5 g sodium nitrate NaNO<sub>3</sub> (99.99% Sigma-Aldrich) at temperature about 0 °C, the mixture was put in a water bath for 1 h at 35 °C, and then 50 ml deionized water was added to the mixture. After that 5 mL of 30% hydrogen peroxide H<sub>2</sub>O<sub>2</sub> (36%, Alfa Aesar, Ward Hill, MA, USA) was added and stirred, the precipitated material was separated from the solution by high-speed centrifuge. The graphene oxide, GO, was then formed and washed for several washing cycles, and then dried at about 50 °C. Dispersion process of the resulted GO was completed by sonication in deionized water for about 1 h.

#### **Preparation of GO/Ag NC**

Numerous methods have been reported for synthesizing GO/Ag NC, which involve chemical reduction, thermal reduction, and photochemical reduction. Furthermore, water or ethanol-based GO suspension is permitted to interact with a silver precursor in existence of sodium citrate as reducing agent or polymers to complete the reduction of metal ions to produce GO/Ag NC. A novel and high stable GO/Ag NC was synthesized via the ex-situ method by slow addition of 10 ml of Ag@Cht NPs with 10 ml GO colloid in a beaker glass for 1 h. The volume ratio between GO and Ag@Cht NPs is 1:1. The mixture was homogenized for 30 min under sonication at room temperature conditions. The GO/Ag NC was dried using the lyophilizer.

#### **Laser photostability of Ag@Cht NPs and GO/Ag NC**

The prepared nanomaterials were exposed to (diode-pumped solid state) laser beam DPSS of wavelength 405 nm and power 50 mW to investigate the photostability of

these nanomaterials. The indicator of tracking any change of these nanomaterials during the laser exposure is the optical absorption. Prior to exposure, the prepared solutions' absorption spectra were measured, and then they were subsequently exposed to laser light for 2, 4, 6, and 8 min exposure times.

#### **Characterization of GO, Ag@Cht NPs and GO/Ag NC**

Absorbance was measured from 300 to 800 nm using a double-beam UV–Vis–NIR spectrophotometer (Cary 5000, Agilent, Santa Clara, USA) with quartz cuvette. The morphology of the prepared nanomaterials as well as their internal structure were examined using a high-resolution transmission electron microscope (HRTEM, Tecnai, G20, FEI, Almelo, Netherlands) under accelerating voltage of 200 kV. The samples under investigation by HRTEM have been prepared by dropping a few droplets of the diluted suspensions of the prepared nanomaterials at carbon-coated copper grids and allowed to be dehydrated at room temperature. Raman spectra of nanomaterials were systematically analyzed by (Raman Senterra II, Germany) using a laser beam of wavelength of 532 nm. FTIR measurements were performed using FTIR spectrometer (4100 Jasco-Japan) in the wavenumber range from 4000 to 400  $\text{cm}^{-1}$ . Samples were freeze-dried via SP Scientific (BTP-3ESEOX, England) for measurement.

#### **Cytotoxicity assay**

The sensitivity of selected available cell lines to the prepared nanomaterials was investigated by different concentrations of GO, Ag@Cht NPs and GO/Ag NC for all the tested cell lines. The cell lines most sensitive to the treatment regimen were selected and further studies were performed to investigate the interaction mechanism. A human lung cancer cell line (H460), a human colon cancer cell line (HCT116), a human breast tumor cell line (MDA-MB-468), and a human hypopharyngeal cell line (FaDu) were used in this study. Cells were gained from the American Type Culture Collection (ATCC, Minnesota, USA). Tumor cell lines are deposited at the National Cancer Institute (NCI), Cairo, Egypt. The antitumor activity of the prepared nanomaterials was estimated using the sulforhodamine B (SRB) assay. Cells were cultured in 96-well microtiter plates at a density of  $3 \times 10^3$  cells/well. Before drug incubation, they could stand for 24 h. The cells were then treated with different concentrations of GO, Ag@Cht NPs and GO/Ag NC (200, 400 and 600  $\mu\text{g}/\text{ml}$ )  $\mu\text{g}/\text{ml}$  for (H460), (HCT116), (MDA-MB-468) and (FaDu). Each concentration was administered to three wells, and the incubation process was continued for 48 h. Vehicle control consisted of DMSO (1% v/v). Following growth, cells were dyed with 0.4% SRB dye and fixed with 20% trichloroacetic acid. Utilizing an ELISA microplate reader (TECAN Sunrise TM, Germany) and spectrophotometry at 570 nm, the optical density (OD) of each individual well was determined. The formula used to compute the mean fractional survival to each drug concentration was  $\text{O.D. treated cells}/\text{D.O. control cells}$ . Using soft-wear sigmoidal dose–response curve fitting models, the IC<sub>50</sub> value (concentration causing 50% inhibition of cell growth) for each medication was determined (Graph Pad Prizm v5 software) (Skehan et al. 1990).

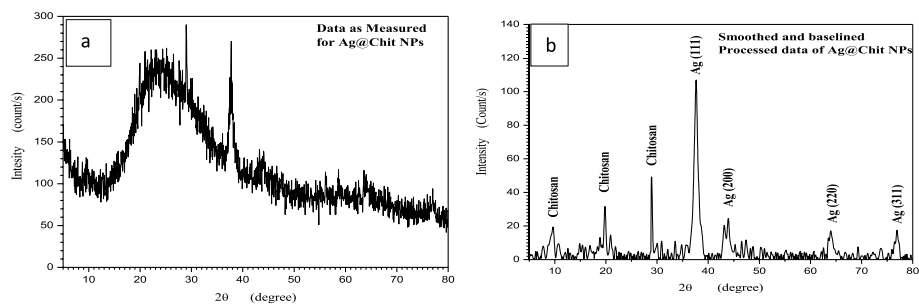


**Fig. 1** XRD patterns of Ag@Chit NC. **a** The as-measured XRD pattern. **b** The processed and identified patterns

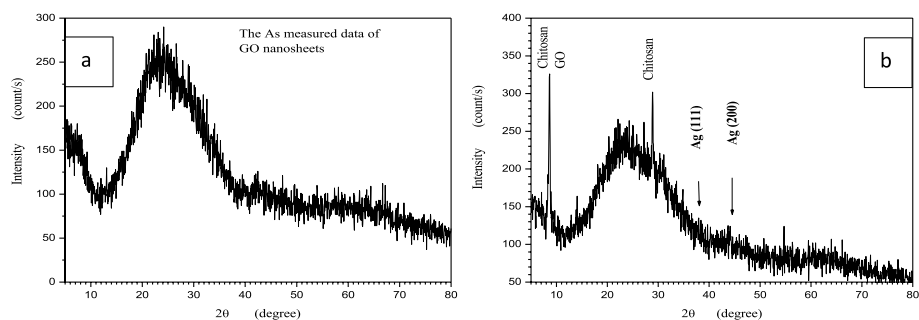


**Fig. 2** XRD patterns of **a** GO **b** GO/Ag@Chit NC

### Statistical analysis

Statistics are presented as mean  $\pm$  SD. Statistical analysis was achieved by means of Graph Pad Prism v5 software. Utilizing Tukey's multiple comparison test, statistical analysis of the transfection test results was carried out. If  $p \leq 0.05$ , differences were statistically significant.

## Results and discussion

### Characterization of Ag@Chit NPs, GO, and GO/Ag NC

There are three prepared nanomaterials that have been under investigation. They are the silver nanoparticles that were prepared using chitosan reduction process, graphene oxide nanosheets that have been prepared using Hummer's method and the composite between them using an ex-situ method (Ramadan et al. 2024; Salah et al. 2023). The crystalline structural characterization has been investigated by X-ray diffraction (XRD) process as follows: first, it is important to mention that chitosan plays two roles in silver salt reduction as well as capping agent. XRD pattern of the silver nanoparticles is represented in Fig. 1. According to few materials, lower crystallinity and nanosized dimensions, the XRD pattern has been processed to eliminate the high-frequency noises, baseline background and peaks identification as shown in Fig. 2. There are two groups of peaks that have been identified. The first group of peaks started from diffracted angle of near  $38^\circ$  that correspond to face-centered cubic structure (FCC) of metallic silver. Identification of crystalline orientations has been done using JCPDS, No 04-0783 standard card of FCC of Ag (Khan and Al-Thabaiti 2022). The second group of three characteristic

peaks at lower angle of the diffraction patterns that belongs to Chitosan semi-crystalline [R1-R2]. The peak profile of the silver diffraction pattern was analyzed using Scherrer's equation to calculate the average crystallite size consisting of each particle:

$$D = \frac{K\lambda}{\beta \cos\theta} \quad (1)$$

where  $D$  is the crystallite size taken from a single diffracted peak,  $K$  is constant equal to 0.9 for particles,  $b$  is the peak width at half-maximum obtained from the peak profile and  $q$  is the half of the diffracted angle obtained from the pattern [R3]. The calculated silver crystallite size ( $D_{Ag}$ ) was averaged over all Ag diffracted peaks which was found to be  $D_{Ag} = 9.4 \pm 0.6$  nm. The chitosan crystallite size ( $D_{Chit}$ ) was also averaged over the chitosan diffracted peaks which was found to be 4.5 nm. XRD measurements of the GO nanosheets are presented in Fig. 2. GO is characterized by two diffracted peaks below  $10^\circ$  and near  $26.8^\circ$ . These two peaks disappeared and new one is generated at  $24.5^\circ$  when a reduction process occurs in GO [R4, R5, R6]. In our sample, a broad hump is presented in Fig. 2a, with two very weak peaks that are hardly to resolved using the software processing of the pattern, but they can be hardly recognized in the as-measured data of Fig. 2a. Figure 2b represents the XRD pattern of the composite of GO with chitosan-capped silver nanoparticles. The as-measured data show two strong diffracted peaks. The first one is at angles below  $10^\circ$  which corresponds chitosan or GO, while the second one near  $30^\circ$  which correspond to the chitosan. The other peaks are belonging to silver nanoparticles, while their intensities are very small. Structural investigation of the prepared nanomaterials and nanocomposites confirms that the formation of both silver nanoparticles of size below 10 nm and smaller particles of size below 5 nm are included in the system in separate crystalline phase which is a composite with the silver nanoparticles (Soomro et al. 2018; Abed, et al. 2021). In addition, both graphene oxide as well as nanocomposite by silver nanocomposite were also confirmed. Besides, the chitosan–silver nanocomposite average diameter does not exceed the sum of their crystallite sizes ( $4.5 + 9.5 = 14$  nm), when each particle contains single crystallite oriented in preferred phase (Zheng et al. 2016).

The three nanomaterials have been dropped at a carbon-coated copper grids to investigate their bulk and microstructure using TEM as represented in Fig. 3a, b and d. The GO TEM image shown in Fig. 3a represents no morphological features except for different zones thickness with some cracks. Each zone has different thickness in the gray scale due to several GO sheets of different numbers for each zone. TEM images of both Ag@Chit nanoparticles and GO/Ag@Chit nanocomposite are represented in Fig. 3b and d. The image of Fig. 3b represents monodispersed dark spheres of Ag@Chit NPs, while those nanoparticles are bounded to each other on a very thin sheets in Fig. 3d, due to nanocomposite of those nanoparticles with GO. The spacings of the non-agglomerated Ag@Chit NPs are much higher than their sizes. Statistical analysis of the particle sizes in the two TEM images are represented in Fig. 3c and e. The normal distribution behavior of the particle size is dominant for the size distribution of the nanoparticles of the Ag@Chit NPs and GO/Ag@Chit NC with average size of 12.8 nm and 14.2 nm, respectively. The average nanoparticles sizes in both free Ag@Chit NPs and composite GO nanoparticles are quite higher for those

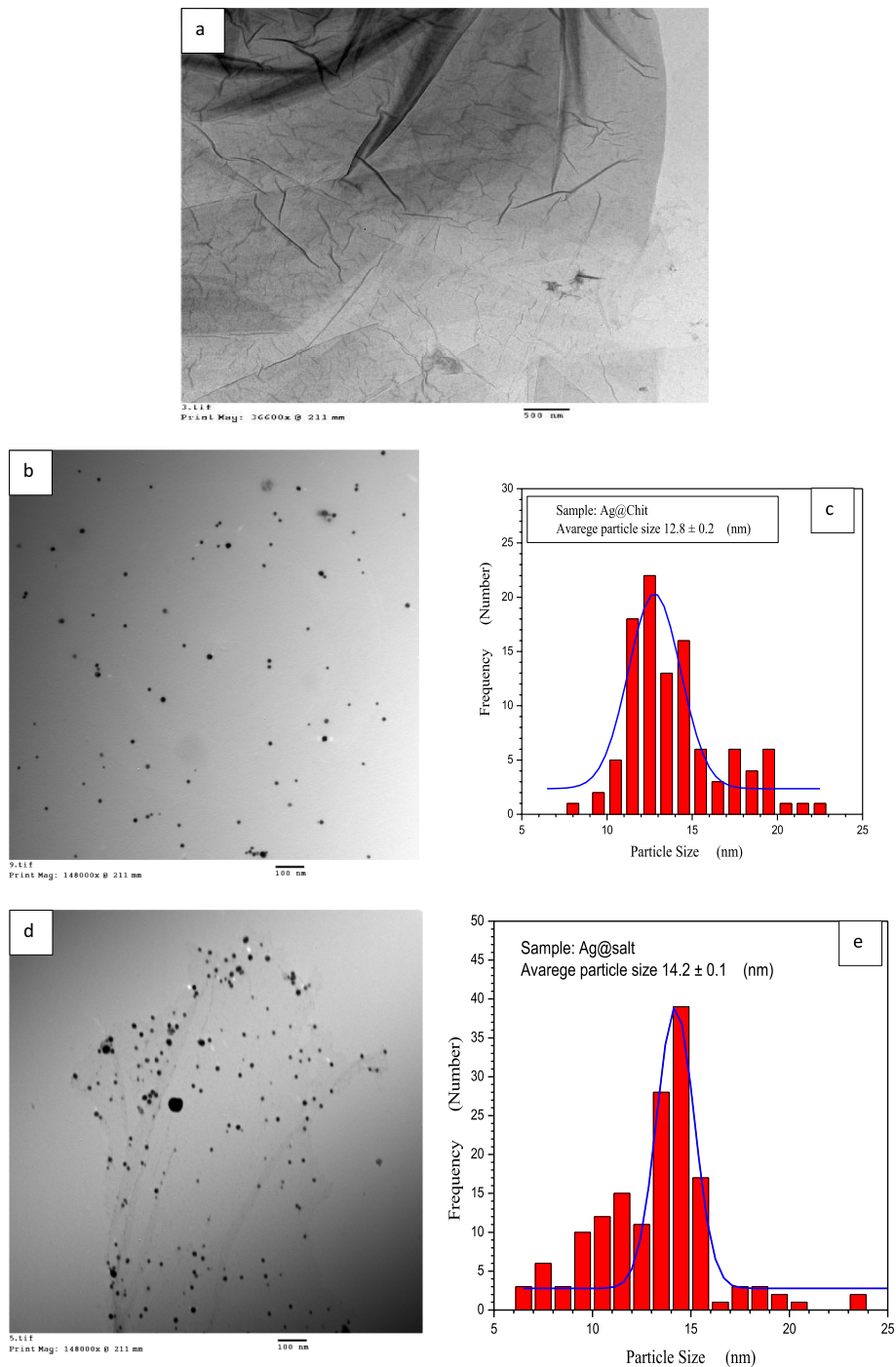


**Fig. 3** **a** TEM image for GO, **b** Ag@Chit NPs, **c** particle size distribution analysis **d** GO/Ag NC and **e** particle size distribution analysis

obtained from XRD profile analysis which indicates that the appeared nanoparticles in the images include the chitosan-capped silver nanoparticles Ag@Chit NPs and their size are the sum of their crystallite sizes. Both Ag@Chit NPs and GO/Ag@Chit NC have limited few bigger size in TEM images than XRD that do not exceed 22 nm



and 28 nm, respectively. These difference in average particle sizes and the limited nanoparticles indicate the higher selectivity in compositing of bigger nanoparticles by GO; this result is directly deduced from the normal distribution of nanoparticles that the distribution becomes narrower in the GO compositing process, while the distribution becomes wider for free Ag@Chit NPs. These structural and microstructural notes evaluate the chitosan reduction and capping process for monodispersed Ag@Chit NPs besides supporting the resultant capped nanoparticles on GO which can be considered as green synthesis of GO/Ag@Chit NC.

The digital pictures of a suspension of the prepared nanomaterials GO, Ag@Chit NPs and GO/Ag@Chit NC are filled in quartz cuvettes and are shown in Fig. 4a. The solutions in the three cuvettes are clear and homogenous with GO suspension is white yellowish, while both Ag@Chit NPs and their composite are brown. The nanocomposite seems to be darker than the silver nanoparticles. The optical absorbance measurement of the suspended GO, Ag@Chit NPs and GO/Ag@Chit NC are represented in Fig. 4b. The GO main characteristic peak appears near UV region in the range 225 and 280 nm. This peak is too broad to be divided into two unresolvable peaks that are equivalent to the aromatic C–C bonds of the  $\pi$ – $\pi^*$  transitions and C=O bonds of  $n$ – $\pi^*$  transitions as discussed by Salah et al. (2023). The absorbance spectra of the suspended Ag@Chit NPs have two peaks, the first in the wavelength range 225–230 nm with sharp absorption edge. This absorption peak is quite different from the absorption peak of the GO because the Ag@Chit NPs is not yet composited with Go. The other peak is observed to be broad with maximum at 427 nm which was characterized by the surface plasmon resonance (SPR) band of Ag@Chit NPs. The optical absorbance of the GO/Ag@Chit NC (the blue curve) has also two peaks in both UV (near 230 nm) which overlap between GO or chitosan, because they are close to each other while the characteristic broad peak near 425 nm was observed to be blue shifted by few nanometers as a result of GO decorated Ag@Chit nanoparticles. The blue shift in optical absorption is due to the reduction in particle size according to GO size selectivity which is discussed in the structural investigations by TEM particles distribution and XRD of the Ag@Chit NPs and nanocomposite GO/

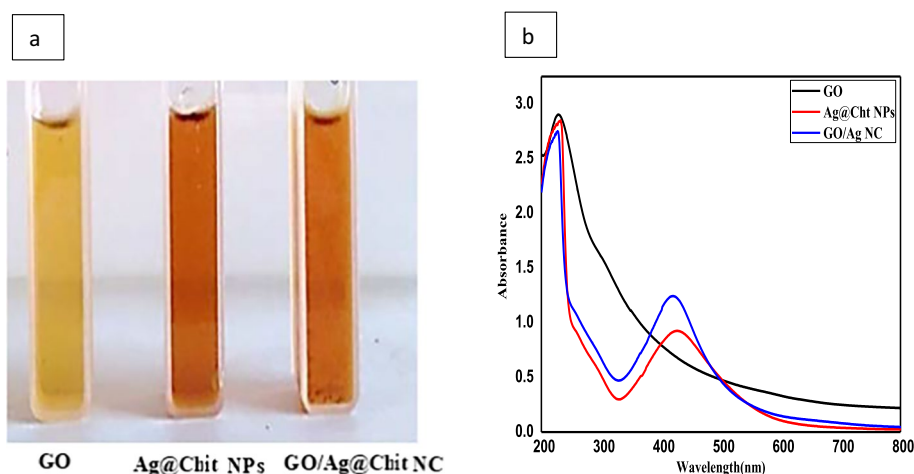


**Fig. 4** UV–visible absorbance of **a** digital photograph of the prepared samples. **b** GO, Ag@Chit NPs and GO/Ag NC

Ag@Chit NC by the narrower particles selectivity using GO nanosheets. Furthermore, Ag@Chit NPs interact with the GO nanosheets by an electrostatic binding without significantly aggregating. The GO sheets serve as an effective support and stabilizer for the Ag@Chit NPs with high selectivity towards the smaller and uniform of particle size (Liu et al. 2011; Lu et al. 2009). The data obtained of the optical absorbance for both three nanostructures agree well with earlier published work by Shujahadeen et al (2017).

**Photostability of Ag@Chit NPs and GO/Ag NC**

The use of Ag@Chit NPs and GO/Ag NC in the treatment of cancer makes the requirement for photostability significant. Cells will be exposed to laser light when it is decided to use these particles as hyperthermic agents in photothermal therapy. Ag@Chit NPs and GO/Ag NC must be exposed to laser light for (0, 2, 4, 6 and 8 min) to be tested for stability. According to Fig. 5a and b, exposing Ag@Chit NPs and GO/Ag NC to DPSS (diode-pumped solid state) laser radiation for various durations did not impact on the particles’ surface plasmon resonance (SPR), which indicates the prepared nanomaterials’ photothermal stability.

Figure 6a shows FTIR spectra for chitosan and silver reduced by chitosan. Different bands in the GO spectrum are connected to various oxygen-containing functional

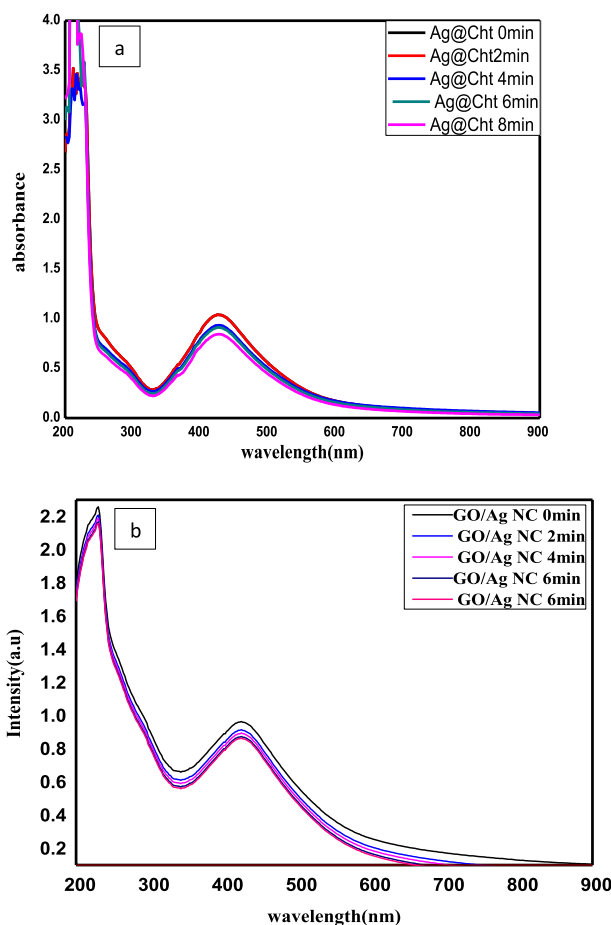


**Fig. 5** Effect of DPSS laser irradiation on **a** Ag@Chit NPs and **b** GO/Ag NC for (2, 4, 6 and 8 min)

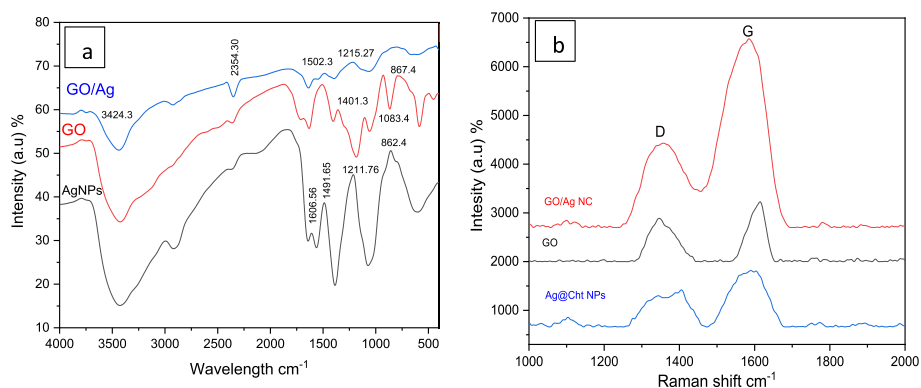


**Fig. 6** **a** FTIR spectra of GO, Ag@Cht NPs and GO/Ag NC. **b** Raman spectra of GO, Ag@Cht NPs and GO/Ag NC

**Table 1** Raman shift and intensity ratio of GO, Ag@Cht NPs and GO/Ag NC

Samples	D ( $\text{cm}^{-1}$ )	G ( $\text{cm}^{-1}$ )	I <sub>D</sub> /I <sub>G</sub>	L <sub>a</sub> (nm)
GO	1353.39	1599.17	1.55849	10.7823
GO/Ag	1363.42	1604.19	1.0016	16.77725
Ag@Cht	1379.73	1587.89	0.76695	21.91041

groups' vibrational modes. A broadband within 3400–3000  $\text{cm}^{-1}$  was due to the –OH stretching vibration mode of the carboxylic moiety (and residual water). The absorption bands at 2930  $\text{cm}^{-1}$  and 2850  $\text{cm}^{-1}$  correspond to the –CH<sub>2</sub>– stretching vibration. The peak at C=O linkages in carboxylic acid and carbonyl moieties is what causes the band at 1726  $\text{cm}^{-1}$  to exist that result from the stretching vibration of C–O in carboxylic acid and carbonyl moieties. The peak at 1606  $\text{cm}^{-1}$  is attributed to the stretching deformation vibration of intercalated water or the skeletal vibrations of unoxidized graphitic domains (Rodríguez-González et al. 2016). The peaks corresponding to aromatic C=C bending, phenolic C–O stretching and epoxy C–O–C stretching were identified at 1200, 1083.7 and 1020  $\text{cm}^{-1}$ , respectively (Rodríguez-González et al. 2016; Cobos et al. 2020). For the GO/Ag NC, the decreasing of the intensity of the carbonyl and hydroxyl bands is detected (Gurunathan et al. 2015a, 2015b, 2016). In addition, the shift in peak of GO/Ag NC is due to silver ions and carboxylate groups association on GO nanosheets via formation of a coordination bond or by simple electrostatic attraction. An elimination of the bands at 1083 and 1606  $\text{cm}^{-1}$  was observed. Particularly, the GO/Ag NC reveals a innovative band at 1494  $\text{cm}^{-1}$ , owing to C–N stretching vibration of GO/Ag NC. These results confirm that the formed GO/Ag NC is stabilized by numerous pepsin residues via their amine functional groups and propose the rich oxygen-containing functional groups existing in GO permit the combination of a diversity of metal ions (Khashan et al. 2018).

A common approach for displaying carbon products and revealing the crystal structure of carbonaceous materials is Raman spectroscopy. Raman intensities in double and conjugated carbon–carbon bonds can also be measured as shown in Table 1. Figure 6b shows Raman spectrum which display two representative bands, the G band characterizes E<sub>2g</sub> mode inside aromatic carbon (Gurunathan et al. 2015b; Sangiliyandi et al. 2016), and D band attributable to the in-plane carbon ring breathing mode as mention

in Table 1. Their numerical intensities decrease, and it might be brought on by carbon content consumption. AgNPs and chitosan’s attachment to the GO surface caused both bands to move to lower wavenumbers, suggesting that a partial graphitization may have occurred, producing clusters of graphene inside amorphous carbon. The ID/IG ratio fell to its lowest value of 0.76, as shown in Table 1, which serves as a sign of this. This behavior points to the creation of more sp<sup>2</sup> areas with reduced sizes by means of the decrease in GO produced by the interaction between the AgNPs and GO sheets. Equation (2) may be used to determine the graphene clusters’ crystallite size (L<sub>a</sub>), which is measured in nm:

$$L_a(\text{nm}) = \left(2.4 \times 10^{-10}\right) \lambda^4 \left(\frac{I_D}{I_G}\right)^{-1} \tag{2}$$

where λ is the laser wavelength excitation length of 514.5 nm (Aguila et al. 2015).

**Anticancer effect of GO/Ag nanocomposite on different cancer cell lines**

The outcome of the prepared samples as antitumor nanomaterials, cytotoxicity of GO, Ag@Cht NPs and GO/Ag NC were evaluated against different cancer cell lines (H460), (HCT116), (MDA-MB-468), and (FaDu) cells at different concentrations after 48 h using the SRP assay. Outcomes of the current study exposed that all the tested cell lines were affected by GO, Ag@Cht NPs and GO/Ag NC at (200, 400 and 600 µg/ml), and Table 2 and Fig. 7 show that samples have IC50 on all tested cell lines which is after 48 h. Ag@Cht NPs showed strongest effect in all used cell lines by IC50 of 5.5, 9, 6 and 7.75 µg/ml effect on MDA-MB-468, HCT116, H460 and FaDu cells, respectively, as in Table 2. Our results were in accordance with Sadegh Khorrami et al. (2019) where they found that the free silver nanoparticles prepared by plant extract demonstrate higher levels of cytotoxicity on MCF7 than its composite with GO during the same periods of time.

By reason of their high surface-to-volume ratio and enhanced activity, AgNPs might easily penetrate cells, interact with their components, and disrupt the signaling pathways inside them. AgNPs are thought to interact with mitochondria and interfere with the operation of the cell’s electron transport chain, which raises the level of reactive oxygen species (ROS) (Faid et al. 2023; Ismael et al. 2019). Therefore, it is possible to regard ROS-induced oxidative stress as the primary harmful mechanism of AgNPs against cells. As diseased cells have an aberrant metabolism and a fast rate of reproduction, which makes them more vulnerable, it is hypothesized that the better cytotoxicity of AgNPs in contrast to cancerous cells results from the greatest absorption of nanoparticles by cancer cells (Khorrami et al. 2018; Tunç 2024). In addition, the exposure to Ag@Cht NPs might cause changes in cell shape, a decline in cell viability, an increase in LDH (lactate dehydrogenase) release, and ultimately cell death and necrosis. In addition, internalized Ag@Cht NPs have the

**Table 2** The IC50 breast cancer cell lines after 48 h incubation with Ag@Cht NPs and GO/Ag NC

	MDA-MB-468		HCT		FADU		H460	
	IC50	SD	IC50	SD	IC50	SD	IC50	SD
Ag@Cht NPs	5.5	0.26	9	0.44	7.75	0.37	6	0.29
GO/Ag NC	39	1.30	60	4.00	58	3.00	41	7.00

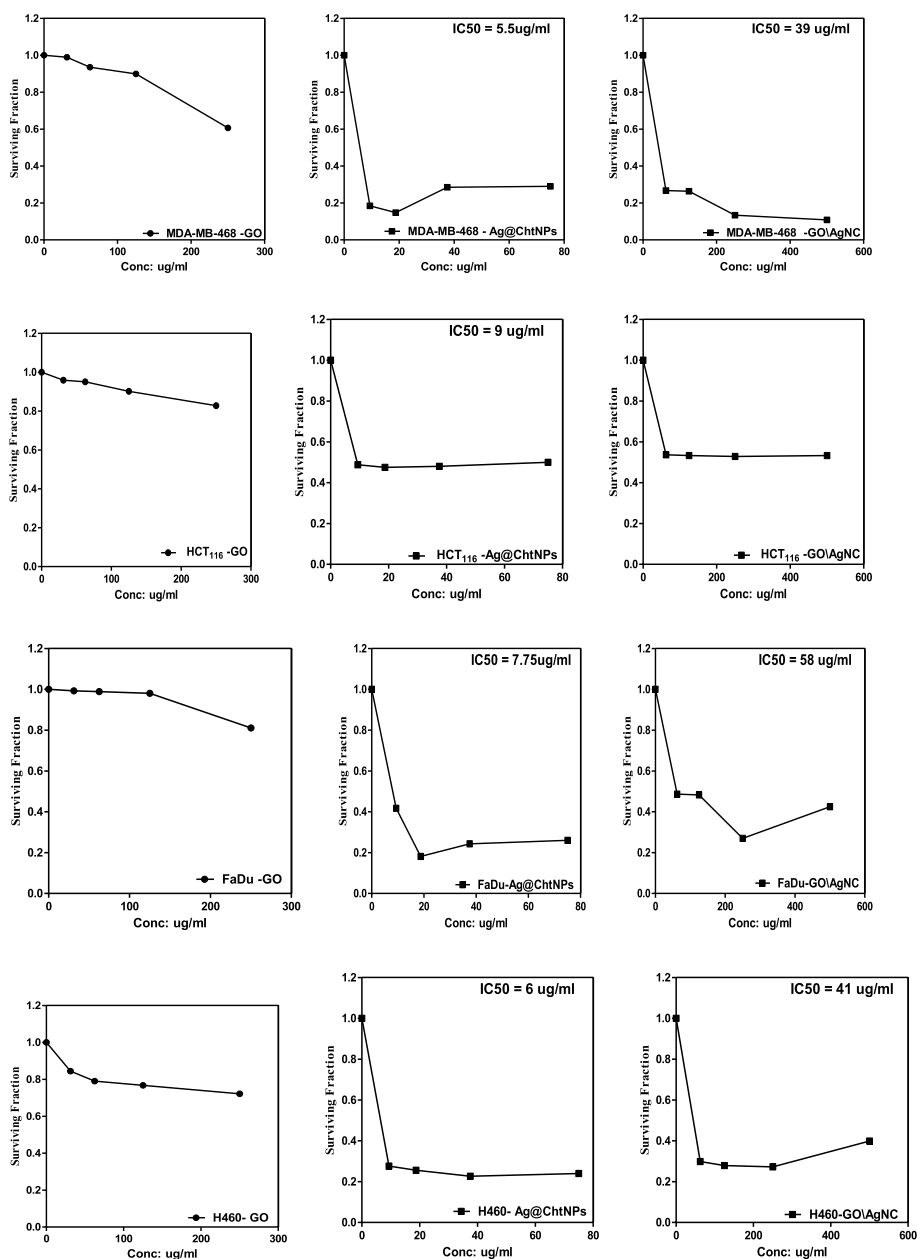


**Fig. 7** SRP-based cell viability assay after 48 h, cell lines were treated with (200,400 and 600  $\mu\text{g/ml}$ ) of Ag@Cht NPs, GO/Ag NC

ability to rupture lysosomal membranes, enlarge lysosomes, and affect the integrity of cell membranes (Abaza et al. 2018). According to several reports, binding GO to other nanoparticles or compounds boosts its effectiveness. Solubility, biocompatibility, dispersion in tumor tissue, and anticancer activities are increased when Ag@Cht NPs are bound to GO (Chen et al. 2023). According to earlier research, the cytotoxicity of quinoline derivatives and GO is caused by cell cycle arrest and apoptosis (Kheiltash et al. 2020; El-Zahed et al. 2021). The outcomes were in agreement with Mariadoss et al. (2020), and they found that

GO-Ag nanocomposite decrease cell viability via ROS, nuclear injury, and mitochondrial membrane potential damage (Mariadoss et al. 2020).

## Conclusion

To conclude, we reported a green sustainable protocol for the development of AgNPs decorated GO, as a high surface area carbonaceous nanocomposite. The biosynthesis was executed using chitosan as the green reducing and capping agent. The synthesized Ag@Cht was dispersed over the high surface of GO. The material was then characterized using various techniques. The formed GO/Ag NC was decorated with well-dispersed spherical shaped AgNPs. Thus, the obtained nanocomposite consists of AgNPs around ~ 15 nm uniformly decorated on GO sheets, which could prevent the agglomeration of the Ag@Cht NPs and open a path for biomedical applications. Raman spectrum displays two representative bands: the G band characterizes E<sub>2g</sub> mode inside aromatic carbon and D band is attributable to the in-plane carbon ring breathing mode; their numerical intensities decrease, and it might be brought on by carbon content consumption.

GO/Ag NC exhibited anticancer toward different cancer cell lines (H460), (HCT116), (MDA-MB-468), and (FaDu) cells at different concentrations after 48 h using the SRP assay. Upcoming work is under way to study the encouraging effects of the prepared novel green synthesized graphene oxide silver nanocomposite for drug delivery, photothermal therapy and chemo-photothermal combination treatment on different cell lines and in vivo study.

## Acknowledgements

The authors extend their appreciation to the Deputyship for Research & Innovation, Ministry of Education in Saudi Arabia for funding this research through the project number IFP-IMSIU-2023040. The authors also appreciate the Deanship of Scientific Research at Imam Mohammad Ibn Saud Islamic University (IMSIU) for supporting and supervising this project.

## Author contributions

MAR and AHF planned and achieved the experiments, analyzed the data. SG and MAR assisted in the materials preparation, optical and structural characterization using UV-Vis, TEM, FTIRs and Raman measurements and MS performed the cytotoxicity experiment. MAR and AHF wrote the manuscript in consultation with MAR, SG, and MS. All the authors read and permitted the final manuscript.

## Funding

Deputyship for Research & Innovation, Ministry of Education in Saudi Arabia for funding this research via the project number IFP-IMSIU-2023040.

## Availability of data and materials

Not applicable.

## Declarations

### Ethics approval and consent to participate

Not applicable.

### Consent for publication

Not applicable.

### Competing interests

All the authors have no competing interests.

Received: 26 January 2024 Accepted: 26 February 2024

Published online: 09 March 2024

## References

- Abaza A, Mahmoud G, Hegazy ES et al (2018) Cytotoxic effect of chitosan based nanocomposite synthesized by radiation: in vitro liver and breast cancer cell line. *J Pharm Pharmacol* 6:89
- Abed M, Mutlak F, Ahmed A et al (2021) Synthesis of Ag/Au (core/shell) nanoparticles by laser ablation in liquid and study of their toxicity on blood human components. *J Phys* 1795:012013

- Aguila S, Shimomoto D, Ipinza F et al (2015) A biosensor based on *Corioliopsis gallica* laccase immobilized on nitrogen-doped multiwalled carbon nanotubes and graphene oxide for polyphenol detection. *Sci Technol Advan Mater* 16:89
- Ahamed M, Akhtar MJ, Khan MAM et al (2021) A novel green preparation of Ag/RGO nanocomposites with highly effective anticancer performance. *Polymers* 13(19):3350
- Ahmed AH, Badr YAE (2018) Improvement of 6-mercaptopurine Efficiency by Encapsulated in Chitosan Nanoparticles. *Arab J Nucl Sci Appl* 51(4):181–186
- Alexeree SMI, Abou-Seri HM, El-Din HES et al (2024) Green synthesis of silver and iron oxide nanoparticles mediated photothermal effects on *Blastocystis hominis*. *Lasers Med Sci* 39(1):43
- Ali MM, Ramadan MA, Ghazawy NA et al (2022) Photochemical effect of silver nanoparticles on flesh fly larval biological system. *Acta Histochem* 124:1–10
- Amin RM, Mohamed MB, Ramadan MA et al (2009) Rapid and sensitive microplate assay for screening the effect of silver and gold nanoparticles on bacteria. *Nanomedicine* 4(6):637–643
- Aziz S, Abdullah O, Saber D et al (2017) Investigation of metallic silver nanoparticles through UV-Vis and optical micrograph techniques. *Int J Electrochem Sci* 12:363–373
- Carrion CC, Nasrollahzadeh M, Sajjadi M et al (2021) Lignin, lipid, protein, hyaluronic acid, starch, cellulose, gum, pectin, alginate and chitosan-based nanomaterials for cancer nanotherapy: challenges and opportunities. *Int J Biol Macromol* 178:193–228
- Chen W, Huang L, Zhou B (2023) Green supported silver nanoparticles over modified reduced graphene oxide: Investigation of its antioxidant and anti-ovarian cancer effects. *Open Chem* 21(1):89
- Cobos M, De-La-Pinta I, Quindós G et al (2020) Graphene oxide-silver nanoparticle nanohybrids: synthesis, characterization, and antimicrobial properties. *Nanomaterials* 10(2):376
- El-Zahed MM, Baka ZA, Abou-Dobara MI et al (2021) In vivo toxicity and antitumor activity of newly green synthesized reduced graphene oxide/silver nanocomposites. *Bioresour Bioprocessing* 8(1):44
- Faid H, Mostafa EM, Ramadan MA (2022) Improved anticancer activity of doxorubicin gold nanohybrid on breast cell line. *Int J Advan Eng Civil Res* 2(1):36–47
- Faid AH, Shouman SA, Badr YA et al (2022a) Enhanced photothermal heating and combination therapy of gold nanoparticles on a breast cell model. *BMC Chem* 16(1):66
- Faid AH, Shouman SA, Thabet NA et al (2022b) Laser enhanced combinatorial chemo-photothermal therapy of green synthesis gold nanoparticles loaded with 6mercaptopurine on breast cancer model. *J Pharm Innov* 34:56
- Faid AH, Hussein FEZ, Mostafa EM et al (2023) Hybrid chitosan gold nanoparticles for photothermal therapy and enhanced cytotoxic action of 6-mercaptopurine on breast cancer cell line. *Beni-Suef Univ J Basic Appl Sci* 12(1):83
- Gurunathan S, Han JW, Kim ES et al (2015a) Reduction of graphene oxide by resveratrol: A novel and simple biological method for the synthesis of an effective anticancer nanotherapeutic molecule. *Int J Nanomed* 10:2951–2969
- Gurunathan S, Han JW, Park JH et al (2015b) Reduced graphene oxide-silver nanoparticle nanocomposite: a potential anticancer nanotherapy. *Int J Nanomed* 10:6257–6276
- Gurunathan S, Park J, Choi Y et al (2016) Synthesis of graphene oxide-silver nanoparticle nanocomposites: an efficient novel antibacterial agent. *Curr Nanosci* 12:762–773
- Hong W, Bai H, Xu Y et al (2010) Preparation of gold nanoparticle/graphene composites with controlled weight contents and their application in biosensors. *Phys Chem C* 114:1822–1826
- Iravani S, Varma RS (2020) Green synthesis, biomedical and biotechnological applications of carbon and graphene quantum dots. *A Review Environ Chem Lett* 18(3):703–727
- Ismael I, Taqi Z, Abdul Hussein A et al (2019) Graphene nanoparticles induces apoptosis in MCF-7 cells through mitochondrial damage and NF-KB pathway. *Mater Res Expr* 6:095413
- Khan Z, Al-Thabaiti SA (2022) Chitosan capped silver nanoparticles: adsorption and photochemical activities. *Arab J Chem* 15(11):104154
- Khashan KS, Jabir MS, Abdulameer FA (2018) Preparation and characterization of copper oxide nanoparticles decorated carbon nanoparticles using laser ablation in liquid. *J Phys: Conf Ser* 1003(1):012100
- Kheiltash F, Parivar K, Hayati Roodbari N et al (2020) Effects of 8-hydroxyquinoline-coated graphene oxide on cell death and apoptosis in MCF-7 and MCF-10 breast cell lines. *Iran J Basic Med Sci* 23(7):871–878
- Khorrami S, Zarrabi A, Khaleghi M et al (2018) Selective cytotoxicity of green synthesized silver nanoparticles against the MCF-7 tumor cell line and their enhanced antioxidant and antimicrobial properties. *Int J Nanomed* 13:8013–8024
- Khorrami S, Abdollahi Z, Eshaghi G et al (2019) An improved method for fabrication of Ag-GO nanocomposite with controlled anti-cancer and anti-bacterial behavior; a comparative study. *Sci Rep* 9(1):9167
- Kumari S, Sharma P, Yadav S et al (2020) A Novel Synthesis of the Graphene Oxide-Silver (GO-Ag) Nanocomposite for Unique Physicochemical Applications. *ACS Omega* 5(10):5041–5047
- Lange A, Sawosz E, Wierzbicki M et al (2022) Nanocomposites of graphene oxide-silver nanoparticles for enhanced antibacterial activity: mechanism of action and medical textiles coating. *Materials* 15(9):45
- Liu L, Liu J, Wang Y et al (2011) Facile synthesis of monodispersed silver nanoparticles on graphene oxide sheets with enhanced antibacterial activity. *New J Chem* 35(7):1418–1423
- Liu L, Ma Q, Cao J et al (2021) Recent progress of graphene oxide-based multifunctional nanomaterials for cancer treatment. *Cancer Nanotechnol* 12(1):18
- Lou XW, Yuan C, Archer LA (2006) An unusual example of hyperbranched metal nanocrystals and their shape evolution. *Chem Mater* 18(17):3921–3923
- Lozovskis P, Jankauskaitė V, Guobienė A et al (2020) Effect of Graphene Oxide and Silver Nanoparticles Hybrid Composite on *P aeruginosa* Strains with Acquired Resistance Genes. *Int J Nanomed* 15:5147–5163
- Lu G, Mao S, Park S et al (2009) Facile, noncovalent decoration of graphene oxide sheets with nanocrystals. *Nano Res* 2(3):192–200
- Mariadoss AVA, Saravanakumar K, Sathiyaseelan A et al (2020) Preparation, characterization and anti-cancer activity of graphene oxide-silver nanocomposite. *J Photochem Photobiol B* 210:111984

- Mohamad EA, Rageh M, Ezz-Aldoula RA et al (2023a) Examination of the interaction between bovine albumin and gold nanoparticles. *Egypt J Chem* 78:1689–1694
- Mohamad EA, Ramadan MA, Mostafa MM et al (2023b) Enhancing the antibacterial effect of iron oxide and silver nanoparticles by extremely low frequency electric fields (ELF-EF) against *S. aureus*. *Electromagn Biol Med* 90:1–15
- Mostafa MM, Mohamad EA, Ramadan MA et al (2022) Reduced Graphene Oxide @ Magnetite Nanocomposite and ELFEF effect on *Staphylococcus aureus* growth inhibition. *Egypt J Chem* 56:267–278
- Motafeghi F, Gerami M, Mortazavi P et al (2023) Green synthesis of silver nanoparticles, graphene, and silver-graphene nanocomposite using *Melissa officinalis* ethanolic extract: Anticancer effect on MCF-7 cell line. *Iran J Basic Med Sci* 26(1):57–68
- Nasrollahzadeh M, Atarod M, Jaleh B et al (2016) In situ green synthesis of Ag nanoparticles on graphene oxide/TiO<sub>2</sub> nanocomposite and their catalytic activity for the reduction of 4-nitrophenol, congo red and methylene blue. *Ceram Int* 42(7):8587–8596
- Ramadan MA, El-Tayeb TA (2023) Photostability, cytotoxicity, and photothermal impact of AgNPs, CoAgNC, and IOAgNC on HEP-2 laryngeal carcinoma cells. *SN Appl Sci* 5(9):253
- Ramadan MA, Sharaky M, Faid AH (2022) Ionic gelation synthesis, characterization and cytotoxic evaluation of chitosan nanoparticles on different types of human cancer cell models. *Egypt J Chem* 65(2):153–159
- Ramadan MA, Sharaky M, Gad S, et al., Anticancer effect and laser photostability of ternary graphene oxide/chitosan/silver nanocomposites on various cancer cell lines. *Nanomedicine (Lond)*, 2024.
- Raza S, Ansari A, Siddiqui NN et al (2021) Biosynthesis of silver nanoparticles for the fabrication of non cytotoxic and antibacterial metallic polymer based nanocomposite system. *Sci Rep* 11(1):10500
- Rodríguez-González C, Velázquez-Villalba P, Salas P et al (2016) Green synthesis of nanosilver-decorated graphene oxide sheets. *IET Nanobiotechnol* 10(5):301–307
- Sajjadi M, Nasrollahzadeh M, Jaleh B et al (2021) Carbon-based nanomaterials for targeted cancer nanotherapy: recent trends and future prospects. *J Drug Target* 29(7):716–741
- Salah A, Hassab-Elnaby S, Ramadan MA (2023) Boosting the nonlinear optical absorption of graphene oxide, and gold nanorods by tailoring graphene oxide-gold nanorods hybrids. *SN Appl Sci* 5(11):288
- Samah AL, Taher AS, Marwa AR et al (2017) Synthesis, Characterization and Cytotoxic Evaluation of Graphene Oxide Nanosheets. *In Vitro Liver Cancer Model. Asian Pac J Cancer Prev* 18:955–961
- Sangilyandi G, JungHyun P, Yun-Jung C et al (2016) Synthesis of Graphene Oxide-Silver Nanoparticle Nanocomposites: An Efficient Novel Antibacterial Agent. *Curr Nanosci* 12(6):762–773
- Skehan P, Storeng R, Scudiero D et al (1990) New colorimetric cytotoxicity assay for anticancer-drug screening. *J Natl Cancer Inst* 82(13):1107–1112
- Soomro S, Gul I, Naseer H et al (2018) Improved performance of CuFe<sub>2</sub>O<sub>4</sub>/rGO nanohybrid as an anode material for lithium-ion batteries prepared via facile one-step method. *Curr Nanosci* 14:90
- Tao F, Cheng Y, Shi X et al (2020) Applications of chitin and chitosan nanofibers in bone regenerative engineering. *Carbohydr Polym* 230:115658
- Tramonti V, Lofrumento C, Martina MR et al (2022) Graphene oxide/silver nanoparticles platforms for the detection and discrimination of native and fibrillar lysozyme: a combined QCM and SERS approach. *Nanomaterials* 12(4):56
- Tunç T (2024) Synthesis and characterization of silver nanoparticles loaded with carboplatin as a potential antimicrobial and cancer therapy. *Cancer Nanotechnol* 15(1):2
- Xu L, Wang Y-Y, Huang J et al (2020) Silver nanoparticles: Synthesis, medical applications and biosafety. *Theranostics* 10(20):8996–9031
- Yan J, Chen J, Zhang N et al (2020) Mitochondria-targeted tetrahedral DNA nanostructures for doxorubicin delivery and enhancement of apoptosis. *J Mater Chem B* 8(3):492–503
- Yousefi M, Dadashpour M, Hejazi M et al (2017) Anti-bacterial activity of graphene oxide as a new weapon nanomaterial to combat multidrug-resistance bacteria. *Mater Sci Eng C Mater Biol Appl* 74:568–581
- Yuan Y-G, Cai H-Q, Wang J-L et al (2021) Graphene oxide-silver nanoparticle nanocomposites induce oxidative stress and aberrant methylation in caprine fetal fibroblast cells. *Cells* 10(3):682
- Zheng P, Liu T, Su Y et al (2016) TiO<sub>2</sub> nanotubes wrapped with reduced graphene oxide as a high-performance anode material for lithium-ion batteries. *Sci Rep* 6(1):36580

## Publisher's Note

Springer Nature remains neutral with regard to jurisdictional claims in published maps and institutional affiliations.